IEEE Access
Multidisciplinary | Rapid Review | Open Access Journal

SPECIAL SECTION ON DATA ANALYTICS AND ARTIFICIAL INTELLIGENCE FOR PROGNOSTICS AND HEALTH MANAGEMENT (PHM) USING DISPARATE DATA STREAMS

Received November 29, 2019, accepted December 6, 2019, date of publication December 13, 2019,
date of current version December 23, 2019.

Digital Object Identifier 10.1109/ACCESS.2019.2959444

A Novel Approach of Identifying Railway Track Rail's Modal Frequency From Wheel-Rail Excitation and Its Application in High-Speed Railway Monitoring

BOLUN AN[1,2], LIANG GAO[1,2], TAO XIN[1,2], GUORONG XIANG[1,2,3], AND JI WANG[1,2,3]

[1]School of Civil Engineering, Beijing Jiaotong University, Beijing 100044, China
[2]Beijing Key Laboratory of Track Engineering, Beijing 100044, China
[3]Beijing Engineering Research Centre of Rail Traffic Line Safety and Disaster, Beijing 100044, China

Corresponding author: Liang Gao (lgao@bjtu.edu.cn)

This work was supported in part by the National Natural Science Foundation of China under Grant U1734206, Grant 51678047, and Grant 51827813, in part by the Key Laboratory of Roads and Railway Engineering Safety Control (Shijiazhuang Tiedao University), Ministry of Education under Grant STKF201716, and in part by the Research and Development Program of China Railway Corporation under Grant 2017G011.

ABSTRACT High-speed railway track defects such as rail corrugation, wheel polygonal wear, and rail fastener clip failure are closely related to the modal frequency of the track structure. As the operation time increases, the modal parameters of the track structure will change, and it is necessary to know what they are to diagnose the vibration characteristics. Present methods of modal analysis are limited by measuring points and excitations and cannot be used to extract the operational parameters of the railway track. This paper proposes a novel approach using wheel-rail excitations to identify the rail modal frequency from vibration monitoring data. The approach decomposes the rail acceleration after the wheel-rail excitation passes into intrinsic mode functions and extracts their instantaneous frequencies. The modal frequencies of the rail can be identified from the instantaneous frequencies. To demonstrate the feasibility of the approach, the results using the proposed approach are compared with the modal frequencies of the rail identified using the eigensystem realization algorithm. Then the approach is applied to study the influence of the number of wheel-rail excitations and the number of monitoring points on the identification results in high-speed railway ballastless track rail. The paper concludes that the proposed approach can provide a reliable solution for the identification of the operational modal frequency of track rails based on the monitoring data.

INDEX TERMS High-speed railway track, operational modal frequency, synchrosqueezed wavelet transform, variational mode decomposition.

I. INTRODUCTION

High-speed railway (HSR) which has higher requirements on stability, smoothness, and safety than traditional rail transit has become one of the main modes of transportation today. As the service time of the HSR track system increases, defects including rail corrugation, wheel polygonal wear, and fastener clip failure result in severe vibration and noise and thus threaten the HSR operation [1], [2].

Field investigations found that the occurrence of these problems is closely related to the railway line condition. For example, fastener failure occurs on the Wuhan-Guangzhou HSR line, but it does not occur on the Beijing-Tianjin HSR line using the same vehicle and different track; The proportional of wheel polygonal wear in CRH2A vehicles operating on Guiyang-Guangzhou HSR line is larger than that of the Nanning-Guangzhou railway operating the same vehicle. Different track structures have different vibration characteristics. Therefore, these problems are related to the vibration characteristics of the track structure [3], [4]. When the vehicle is running, there are broadband excitations between the wheels and rails, which vibrate the track structure, and the long-term resonance or anti-resonance causes the above problems [5]. As a structural component that

The associate editor coordinating the review of this manuscript and approving it for publication was Jing Lin.

directly contacts with the vehicle, the rail plays an important role in the vehicle-track dynamic interaction. Therefore, to diagnose and analyze the vibration characteristics and find solutions for these problems, the modal parameters (such as modal frequency, modal shape, modal damping ratio, etc.) of the HSR track rail should be figured out.

Researchers have done some research on the identification of track modal parameters using laboratory tests [6], field tests [7]–[10], and numerical analysis [11], [12]. However, they have two common limitations: (1) only track modal parameters of a certain state can be obtained; (2) only track modal parameters of a certain section can be obtained.

Same as all engineering structures, the track rail is also a time-varying structure whose modal parameters, especially the modal frequencies are easily affected by fastener systems and temperature [2], [4]. In terms of performance degradation of vehicle track systems, research considering aging and degradation for maintenance has been carried out [13], which means that research on track rail operational modal parameters is urgently needed. In the engineering field, the extraction of operational modal parameters from sensing systems has become a research hotspot.

Researchers in bridge engineering and other engineering fields have worked on identifying operational modal parameters. Using the polyreference least squares complex exponential method (LSTE) and the stochastic subspace identification method (SSI), Hermans and Vander Auweraer extracted the modal parameters of bridges [14]. Some improved methods based on SSI have been applied to modal parameter identification of bridges and buildings [15]–[17]. A new modal parameter identification method using the free vibration responses of a bridge based on the time domain decomposition technique (TDD) was proposed by Kim *et al.* [18]. Yan and Ren used power spectrum density transmissibility to identify the modal parameters of a five-story building and an arch bridge [19]. Yang *et al.* used an analytical method to derive the dynamic responses of a bridge and identified the damping [20], mode shape [21], and resonance frequency [22] of the bridge based on vehicle excitation. In addition to the above traditional time-domain methods, time-frequency domain methods [23], artificial neural networks (ANN) [24] and Bayesian analysis [25] have been used to identify the modal parameters of bridges. There is some related research in other engineering fields as well. For example, the PolyMAX method was used to identify the modal parameter of a stadium using the excitation of a football game [26]. Based on SSI, the modal parameters and damage of two masonry structures were identified by Ramos *et al.* [27]. Uehara and Sirohi used the natural excitation technique (NExT), eigensystem realization algorithm (ERA), and complexity pursuit to extract the modal properties of a rotor blade [28]. Jiang *et al.* proposed the PolyMAX method to identify the modal parameters of a lightweight and high-speed structure [29]. Operational modal identification based on Bayesian analysis [30], [31] and time-frequency [32] analysis is also widely used in engineering structures. Deep learning and convolutional deep belief networks are also applied to health diagnosis [33], [34].

At this point, there is little research in the field of HSR track engineering. The current monitoring of railway tracks concentrates on track condition diagnosis, state assessment, and prediction using a large amount of data including stress, strain, displacement and acceleration data [35], [36]. This circumstance leads that the theoretical research in the railway field is still staying in the status that the track mechanical model and analysis are carried out using the design parameters. Besides, there are fewer monitoring points in the railway track, and any sensor degradation will increase maintenance cost [37]. We can identify the modal parameters of the track structure and establish the correlation between the monitoring data and the theoretical model to reduce the error.

Some problems should be solved before identify the operational modal parameters of the HSR track. The first one is that different from the above structures, the track rail is a spatially longitudinal and continuous structure; the operational excitations of the track are wheel-rail forces that do not have white noise characteristics, and therefore the conventional modal identification method by using ambient excitations is not feasible. The second one is that there are some objective obstacles in the HSR track, such as the short maintenance time, long track, complexity of field testing (experimenters must communicate with the railway management department, the operation department, and the service department), etc. And also, it is not feasible to set up a large number of sensor measuring points on the HSR track.

Recently, the method of identifying the instantaneous frequency using the dynamic response of a point on the structure has gradually emerged. These methods firstly decompose the multi-component acceleration signals into single-component intrinsic mode functions (IMFs) using the mode decomposition method, and then, identify the instantaneous frequency of the IMFs using time-frequency analysis method. Among all the mode decomposition methods, variational mode decomposition (VMD) [38] is gradually well-known because it can overcome the shortcomings of modal aliasing [39], [40]; Among all the time-frequency analysis method, synchrosqueezed wavelet transform (SWT) [41] is widely used because it can obtain time-frequency distribution curves with high frequency accuracy [42], [43].

This paper proposes a novel approach to identify the rail modal frequency from wheel-rail excitation (MFIM), using the variational mode decomposition and synchrosqueezed wavelet transform methods. We use the approach to process rail acceleration data obtained from track monitoring and identify the modal frequency of the rail.

The paper is organized as follows. Section 2 explains the approach and Section 3 describes a low vibration track model and uses the eigensystem realization algorithm (ERA) to identify the modal frequency of the rail. Then it compares the ERA results with the MFIM results. Section 4 analyzes the influence of the number of wheel-rail excitations and the number of measuring points on the modal frequency

identification and proposes suggestions for the monitoring measuring points.

II. A NOVEL APPROACH OF RAIL MODAL FREQUENCY IDENTIFICATION FROM WHEEL-RAIL EXCITATION

The basic idea of the approach is shown in Fig.1. The first step is to find and extract the rail acceleration after the wheel-rail excitation passes. The second step is to initially identify the order of the IMF of the signal using continuous wavelet transform (CWT) and empirical mode decomposition (EMD). The third step is to decompose the acceleration signal into k-order IMFs using VMD and the fourth step is to identify their instantaneous frequencies. Due to the wide response range of the HSR, when the adjacent two-order modal frequencies are close and their responses are small, IMFs may have multi-components, and it is necessary to return to the second step to decompose the multi-component IMF. If all IMFs are single-component signals, we can carry out the fifth step: extract the instantaneous frequency of each IMF. In the sixth step, the instantaneous frequencies of the rail and the power spectral density are plotted on the stabilization diagram. Finally, we can identify the modal frequency of the rail by combined its instantaneous frequencies with the PSD.

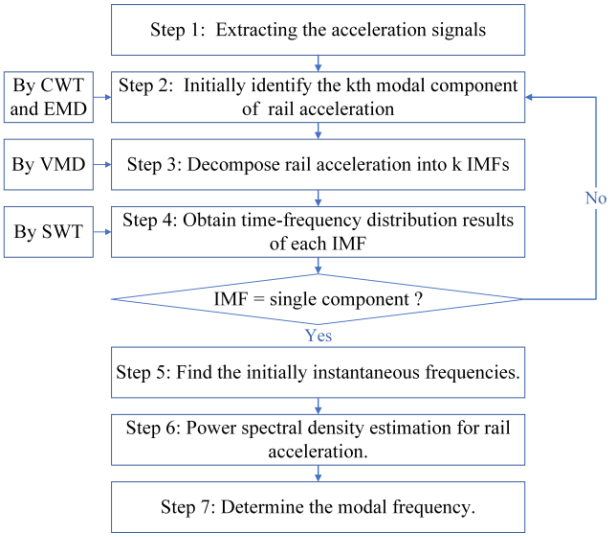

FIGURE 1. Flow chart of MFIM.

The fundamental problem of the approach is whether the influence of wheel-rail excitation can be weakening, and the vibration characteristics of the rail can be extracted. Therefore, it is necessary to analyze the dynamic response of the rail under the wheel-rail excitation. After that, we introduce the VMD and SWT methods.

A. ANALYSIS OF RAIL RESPONSES UNDER THE WHEEL LOAD

The rail is a continuous long-beam structure. Wheel-rail excitations always exist, so in theory, there is no free vibration on the rail. However, because of the elastic support systems below the rail, the rail directly below the wheel has the largest response, whereas farther from the wheel, the response is almost 0. An elastic foundation beam model can be used to analyze the rail response under the wheel load.

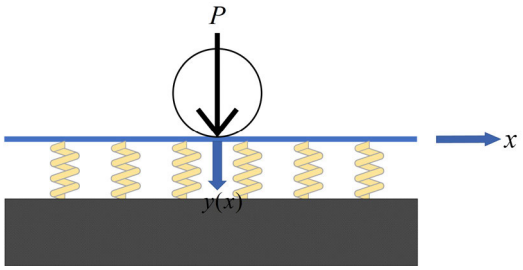

FIGURE 2. Infinite beam on elastic foundation model.

The model of the rail dynamics is shown in Fig.2, and the wheel-rail excitation is considered a moving load. Its dynamic equation of the rail can be expressed as:

$$E_r I\frac{\partial^4 y(x,t)}{\partial x^4}+m\frac{\partial^2 y(x,t)}{\partial^2 t}+c\frac{\partial y(x,t)}{\partial t}+ky(x,t)=0 \quad (1)$$

where E_rI is the bending stiffness of the rail (Nm^2); m is the mass of the rail per meter (kg/m); c is the track damping per meter (Ns/m^2); k is the track stiffness per meter (N/m^2).

Now, we introduce the moving wheel load $Q\delta(x-vt)$ and a dimensionless variable s:

$$s=\lambda(x-vt) \quad (2)$$

where λ can be expressed as $\lambda = 1/\sqrt[4]{E_f/4E_rI_x} = 1/k$ (E_f is the foundation coefficient (kN/cm^2)). An equation about s can be obtained by combining (2) with (1):

$$\frac{d^4y(s)}{ds^4}+4\alpha^2\frac{d^2y(s)}{ds^2}-8\alpha\beta\frac{dy(s)}{ds}+4y(s)=0 \quad (3)$$

in which:

$$\alpha=\frac{v}{2\lambda}\left(\frac{m}{EI}\right)^{\frac{1}{2}} \quad (4)$$

$$\beta=\frac{c}{2m}\left(\frac{m}{k}\right)^{\frac{1}{2}}=\frac{c}{2\sqrt{mk}} \quad (5)$$

where λ is the inverse of k; α is the ratio between actual speed and critical speed, and β is the ratio between actual damping and critical damping.

The solution to (3) can be found in Esveld [44]. The analysis of the displacement response of the rail under the wheel-rail excitation indicates that the rail response is the highest at the position below the wheel ($kx = 0$). When $kx \geq 5$, the effect of wheel-rail excitation on the rail is minimal and, indeed, can be negligible [45].

When vehicles are running on the track, the wheel-rail vibration is large because of various kinds of track irregularities, and the acceleration of the rail below one vehicle wheel can often reach 50g or higher. However, due to the limited range of influence of the wheel loads, after the vehicle passes a certain position on the rail, the forced vibration at that point will decay rapidly, and the free-attenuation vibration will dominate the rail response. The influence of the external

excitation will reduce, and the natural frequency of the rail will be more easily identified. This idea is also applied to discrete structures (such as bridges [18]) to identify the modal parameters of structures.

We compare the rail acceleration after the vehicle passes to the full-time acceleration of the rail to support the above proposal in Section3.

B. VMD METHOD

The main purpose of VMD is to decompose the input signal into a series of mono-component signals. The input multi-component signal is generally composed of k IMFs and can be written as:

$$x(t) = u_1(t) + u_2(t) + \ldots + u_k(t) \tag{6}$$

where $u_k(t)$ is the kth IMF, with a finite frequency bandwidth and center frequency. Each IMF has sparse characteristics in the frequency domain.

In this study, VMD is used to decompose the acceleration of the rail into a series of IMFs, which are then used for the identification of instantaneous frequency by SWT. The main steps of VMD can be expressed by the following equations [34], [35]:

$$\min_{\{u_k\},\{\omega_k\}} \left\{ \sum_k \left\| \partial_t \left(\left(\delta(t) + \frac{j}{\pi t} \right) \times u_k(t) \right) e^{-jw_k t} \right\|_2^2 \right\},$$
$$subject\ to \sum_k u_k = f \tag{7}$$

where $u_k(t)$ and ω_k are the kth IMF and its center frequency, respectively.

The IMF $u_k(t)$ and its center frequency are written as:

$$u_k(\omega) = \frac{f(\omega) - \sum_{i \neq k} u_i(\omega) + (\frac{\lambda(\omega)}{2})}{1 + 2\alpha(\omega - \bar{\omega}_k)^2}, \quad (k = 1, 2, 3, \ldots, K) \tag{8}$$

where $x_p(\omega)$ is the FFT of the signal $x_p(t)$.

Then the steps of the variational problem are the following:

(1) The intrinsic mode update is carried out.
(2) The center frequency of the IMF is updated.
(3) The Lagrangian multiplier is updated.

C. SWT METHOD

The wavelet transform of the signal $x(t)$ can be expressed as:

$$W_x(a, b) = \int_{-\infty}^{\infty} x(t) a^{-\frac{1}{2}} \bar{\psi} \left(\frac{t - b}{a} \right) dt \tag{9}$$

where a is the scale variable; b is the translation variable, and $\bar{\psi}$ is the complex conjugate of the mother wavelet. For any time-scale on the CWT spectrogram, the instantaneous frequency of the signal can be estimated by the wavelet coefficient's derivation:

$$\omega(a, b) = -i \frac{\partial W_x(a, b)}{W_x(a, b) \partial b} \tag{10}$$

where i is the imaginary unit. The wavelet coefficients can be converted from the time-scale domain (b, a) to the time-frequency domain $(b, \omega_x(a, b))$. The next step is to reassign (squeeze) the value of the time-frequency domain result. To do so, the wavelet transform $W_x(a, b)$ is calculated for all the discrete points $a_j(\Delta a_j - a_{j-1})$ in the time-frequency plane. Then the wavelet coefficient is squeezed in a certain frequency range $[\omega_i - \Delta\omega/2, \omega_i + \Delta\omega/2](\Delta\omega = \omega_i - \omega_{i-1})$ around the discrete point. The SWT is defined as [41]–[43]:

$$T_x(\omega_i, b) = \frac{1}{\Delta\omega} \times \sum_{a_j : |\omega(a_j, b) - \omega_i| \leq \frac{\Delta\omega}{2}} W_x(a, b) a_j^{-3/2} (\Delta a)_j \tag{11}$$

At each time scale, the result of (11) makes energy distribution in the time-frequency domain more concentrated.

III. A NUMERICAL EXAMPLE

In this section, we establish a numerical track model to investigate the feasibility of the proposed approach. First, the modal frequency of the model is identified using the ERA method as the control group. Then, the wheel-rail excitation is applied to the track model, and the rail acceleration responses are extracted. The modal frequencies of the rail are identified by MFIM as the studied group.

A. A ESTABLISHMENT OF THE LOW VIBRATION TRACK MODEL

The model (shown in Fig.3) consists of rail, elastic support blocks, fasteners, rubber mats, and wheel-rail loads (as external forces). The rail is considered a simply supported Euler beam, and its equation can be written as follows:

$$EI \frac{\partial^4 Z_r(x, t)}{\partial x^4} + m_u \frac{\partial^2 Z_r(x, t)}{\partial t^2} = -\sum_{i=1}^{N} F_{cbi}(t) \delta(x - x_i) + \sum_{j=1}^{4} p_j \delta(x - x_{wj}) \tag{12}$$

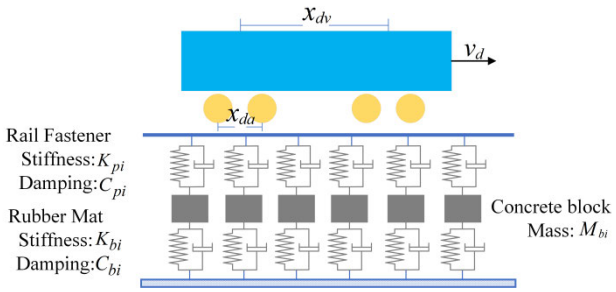

FIGURE 3. Low vibration track model.

where x_j is the position of P_j and can be calculated as:

$$x_j = (t - \Delta t) \times v_d \tag{13}$$

where Δt is the time before the first wheel-rail excitation moves on the beam, and δ is the Dirac function, which can

be expressed as :

$$\delta(x - x_i) = \begin{cases} \infty, & x = x_i \\ 0, & x \neq x_i \end{cases} \tag{14}$$

In the numerical model, we assume that the first wheel enters the track at $t = 1s$; therefore, the location of each wheel can be expressed as:

$$\begin{cases} x_{w1}(t) = \begin{cases} (t-1) \times v, & 1s <= t <= 11s \\ 0, & t < 1s or t > 11s \end{cases} \\ x_{w2}(t) = \begin{cases} (t-1) \times v - x_{da}, & 1.1s <= t <= 11.1s \\ 0, & t < 1.1s or t > 11.1s \end{cases} \\ x_{w3}(t) = \begin{cases} (t-1) \times v - x_{dv}, & 1.6s <= t <= 11.6s \\ 0, & t < 1.6s or t > 11.6s \end{cases} \\ x_{w4}(t) = \begin{cases} (t-1) \times v - x_{dv} - x_{da}, & 1.7s <= t <= 11.7s \\ 0, & t < 1.7s or t > 11.7s \end{cases} \end{cases} \tag{15}$$

where x_{dv} is the length between bogie centers, and x_{da} is the length between the wheel centers. The values of the two parameters are 12.5m and 2.5m, respectively.

The equation of the concrete block can be expressed as:

$$F_{cbi}(t) = K_{pi}[Z_r(x_i, t) - Z_{bi}(t)] + C_{pi}[\dot{Z}_r(x_i, t) - \dot{Z}_{bi}(t)] \tag{16}$$

where $Z_r(x, t)$ denotes the deflection of the rail at time t, and in the position x; N is the number of the fastener (from left); $x_i = ix_{db}$ is the coordinate of the ith support block, where x_{db} is the fastener spacing; $Z_{bi}(t)$ denotes the vertical displacement of the ith elastic support block at time t; F_{cbi} is the force provided by the ith elastic support block; p_j represents the wheel-rail force of the jth wheel. To introduce the regular coordinates of the rail, we apply the regular modal function of the rail:

$$Y_k(x) = \sqrt{\frac{2}{m_u l}} \sin \frac{k\pi x}{l} \tag{17}$$

The solution of (17) can be written as:

$$Z_r(x, t) = \sum_{k=1}^{NM} Y_k(x) q_k(t) \tag{18}$$

We select the rail mode cut-off order NM, substitute (18) into (12), multiply $Y_h(t)$on both sides of the equation, and integrate x from 0 to l, using the orthogonality of the rail to obtain the following equation:

$$\begin{aligned} &\int_0^l EI \frac{d^4 Y_k(x) q_k(t) dx}{dx^4} + \int_0^l m_u Y_k(x) Y_k(x) \ddot{q}(t) dx \\ &= -\sum_{i=1}^{N} \int_0^l F_{cbi}(t) Y_k(x) \delta(x - x_i) dx \\ &\quad + \sum_{j=1}^{4} \int_0^l p_j(t) Y_k(x) \delta(x - x_{wj}) dx \end{aligned} \tag{19}$$

For these:

$$\int_0^l Y_k^2(x) dx = \frac{1}{m_u} \tag{20}$$

$$\begin{aligned} \int_0^l Y_k(x) \frac{d^4 Y_k(x)}{dx^4} dx &= \int_0^l \frac{2}{m_u l} \left(\frac{k\pi}{l}\right)^4 \sin^2 \frac{k\pi x}{l} dx \\ &= \left(\frac{k\pi}{l}\right)^4 \int_0^l Y_k^2(x) dx = \frac{1}{m_u} \left(\frac{k\pi}{l}\right)^4 \end{aligned} \tag{21}$$

Finally, the vibration equation of the rail for the coordinates can be obtained from (19):

$$\begin{aligned} &\ddot{q}_k(t) + \frac{EI}{m_u} \left(\frac{k\pi}{l}\right)^4 q_k(t) \\ &= -\sum_{i=1}^{N} F_{cbi}(t) Y_k(x_i) + \sum_{j=1}^{4} p_j(t) Y_k(x_{wj}) \quad (k = 1 \sim NM) \end{aligned} \tag{22}$$

F_{cbi} can be expressed as:

$$\begin{aligned} F_{cbi}(t) = C_{pi} \sum_{m=1}^{NM} Y_m(x_i) \dot{q}(t) + K_{pi} \sum_{m=1}^{NM} Y_m(x_i) q_m(t) \\ - C_{pi} \dot{Z}_{bi}(t) - K_{pi} Z_{bi}(t) \end{aligned} \tag{23}$$

The vibration equation of a single concrete block is:

$$\begin{aligned} &M_{bi} \ddot{Z}_{bi}(t) + (C_{pi} + C_{bi}) \dot{Z}_{bi}(t) + (K_{pi} + K_{bi}) Z_{bi}(t) \\ &- C_{pi} \sum_{m=1}^{NM} Z_m(x_i) \dot{q}_m(t) - K_{pi} \sum_{m=1}^{NM} Z_m(x_i) q_m = 0, \ (i = 1 \sim N) \end{aligned} \tag{24}$$

The parameters used in the model are shown in Table 1.

TABLE 1. Parameters used in the track model.

Parameter	Symbol	Value
Length of track	l	50 m
Mass per meter of rail	m_u	60 kg
Elastic modulus of rail	E	2.07e11 Pa
Inertia moment of rail	I	30.6e-6 m^4
Fastener spacing	x_{db}	0.625 m
Stiffness of fastener	K_{pi}	30000000 N/m
Damping of fastener	C_{pi}	7500 N·s/m
Mass of elastic block	M_{bi}	110 kg
Stiffness of rubber mat	K_{bi}	20000000 N/m
Damping of rubber mat	C_{bi}	2000 N·s/m
Cutoff mode	NM	40

Two kinds of wheel-rail excitations (shown in Fig.4) with different spectral characteristics are used in the model. Excitation 1 has the following peaks: 2Hz, 10Hz, 30Hz, 45Hz, 58Hz, 175Hz, 292Hz, and 446Hz. Excitation 2 has different peaks: 30Hz, 63Hz, 94Hz, 128Hz, 192Hz, 256Hz, 320Hz, 384Hz, 420Hz, and 448Hz. When the structure is excited

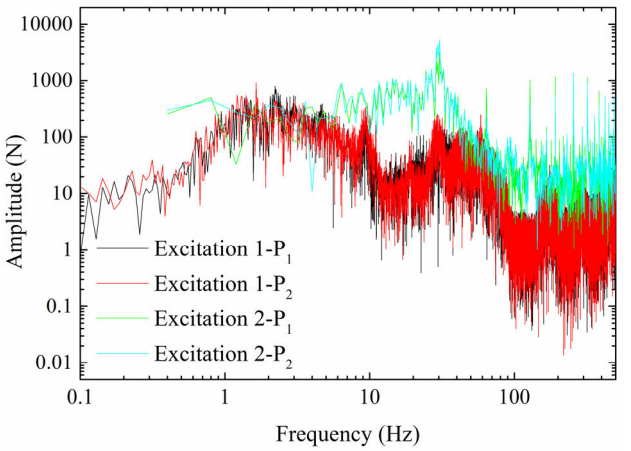

FIGURE 4. Spectrogram of wheel-rail excitations.

by wheel-rail forces, the responses will be affected by these excitations, so the interference of these peaks can be used to examine the accuracy of MFIM.

B. MODAL FREQUENCY IDENTIFICATION BY ERA

From (22)∼(24), we observe that the stiffness matrix and damping matrix of the track model are non-diagonal matrices. It is difficult to obtain the theoretical modal frequency by solving the eigenvalues of the model matrices. Therefore, we use the ERA method [46].

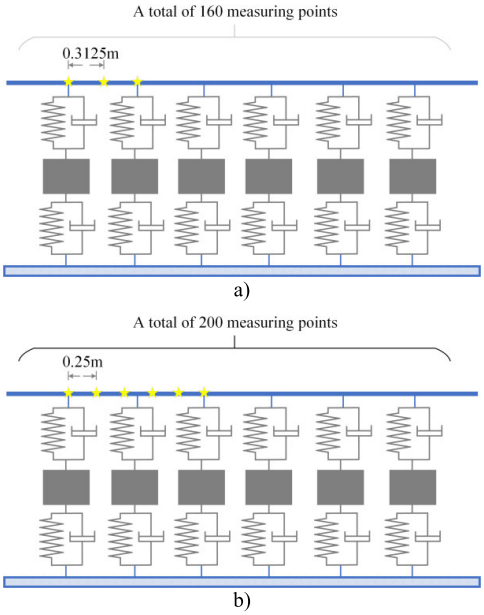

FIGURE 5. The 160 measuring points scheme (a) and the 200 measuring points scheme (b) of the ERA method.

To obtain the rail modal frequency, we use two measuring point scheme conditions. The first condition is set up 159 points, and the rail is equally divided into 160 segments 0.3125m apart (shown as Fig.5(a)). Fourteen measuring points are randomly selected as exciting points. The second condition is set up 199 points (shown in Fig.5 (b)), with 16 measuring points randomly selected as exciting points.

The calculation time is 1s, and the sampling interval is 0.000025s (with the sampling rate of 40000Hz). The pulse excitation force can be expressed as:

$$f(t) = \begin{cases} A\sin(\dfrac{1}{\Delta t} \times \pi \times t), & t \in [0.2, 0.2002] \\ 0, & t \notin [0.2, 0.2002] \end{cases} \quad (25)$$

where A is the amplitude of the excitation, and Δt is the excitation duration.

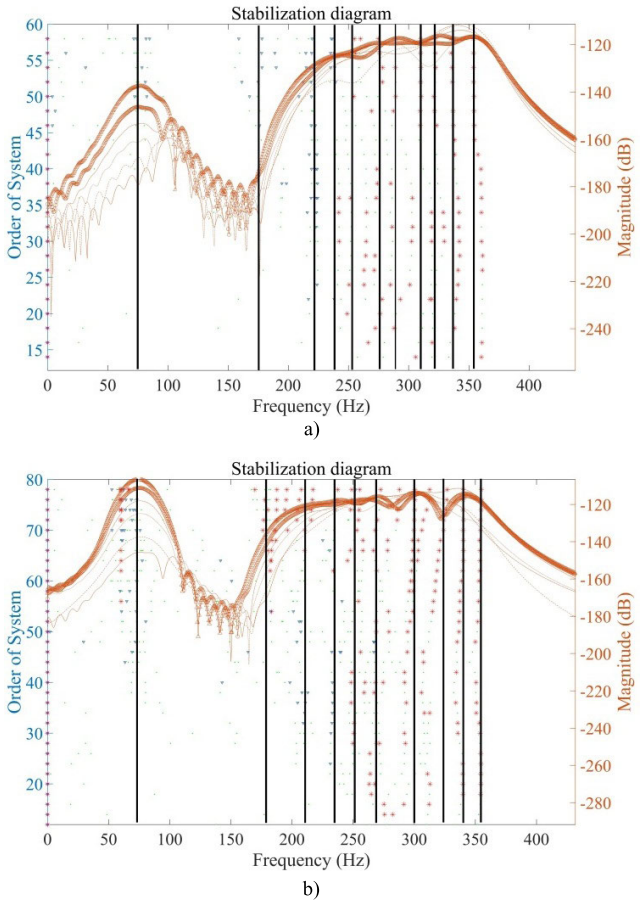

FIGURE 6. Stabilization diagram of the rail under the 160 measuring points (a) and the 200 measuring points (b).

Based on the orange dots (i.e. the frequency, damping, and mode shape are all stable) and blue dots (i.e. that the frequency and damping are stable) and the frequency response functions of the rail, the modal stabilization axes are drawn in Fig.6. If two adjacent modal frequencies are too close (less than 10Hz), then they are considered one mode. Finally, we obtain 11 modal frequencies of the rail. The identification results are shown in Table 3.

C. EFFICACY OF MODAL FREQUENCY IDENTIFICATION USING MFIM

To consider the effect of the excitation speed, we set three conditions (shown in Table 2). The calculation time is 5s, and the sampling frequency is 1000Hz. We extract dynamic responses at three random measuring points on the beam: $0.46875L$, $0.6L$ and $0.8L$ respectively.

TABLE 2. Calculation conditions.

Condition	Wheel-rail excitations	Moving speed
1	Excitation 1	25 m/s
2	Excitation 1	50 m/s
3	Excitation 2	

TABLE 3. Comparison of the ERA method and MFIM.

Modal Order	ERA 1	ERA 2	Condition 1	Condition 2	Condition 3
External Excitation			/		18.8 36.2
1	74.1	72.7	60.9 70.7	60.9 72.2	61.2 76.6
2	175.0	177.9	164.1 182.6	166.2 179.3	191.3
3	221.7	210.9	205.3	204.5	212.5
4	238.6	235.6	/	/	239.7
5	253.3	250.9	/	/	/
6	276.0	268.9	272.1	262.7	274.5
7	289.5	300.1	293.1	282.2/ 295.8	/
8	309.5		307.3	310.4	302.6
9	321.6	324.1	/	/	/
10	336.9	340.1	/	/	/
11	354.6	354.7	/	382.5	341.2
External Excitation	/	/	401.6	412.6	407.2
	/	/	432.2	434.2	443.4
	/	/	/	/	467.2

Fig.7 shows some acceleration results. The signal data after the last wheel passes are extracted to identify the modal frequency of the rail. Fig.8 compares the full-period rail acceleration with the acceleration after the last wheel passes. The blue boxes in the figure represent the peak value of the wheel-rail excitations. As can be seen from the figure that when only the rail acceleration after the last wheel pass is analyzed, the amplitude away from the rail modal frequency (i.e. peak values of 30Hz, 128Hz, 192Hz, 256Hz, 320Hz, 384Hz, and 420Hz) will decrease, whereas the amplitude near the rail modal frequency will increase (peak value 63Hz). This finding is consistent with the analysis in Section2.

First, we use the CWT and EMD method on the acceleration data, and the result shows that the number of IMFs

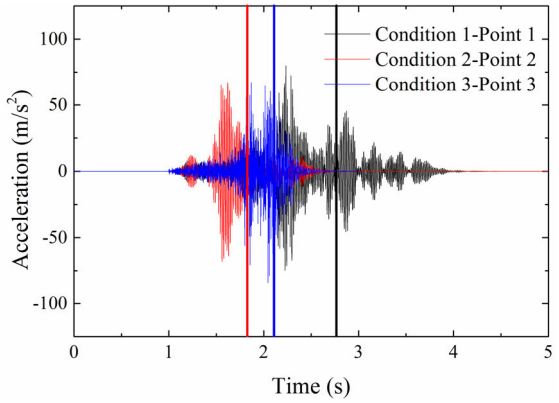

FIGURE 7. Rail acceleration under wheel-rail excitations.

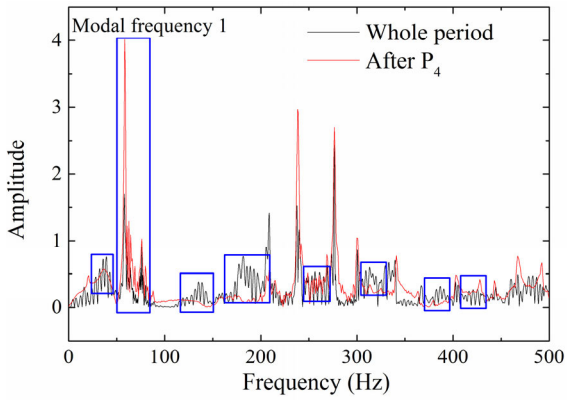

FIGURE 8. Comparison between full period rail acceleration and the acceleration after the last wheel passes.

is 10. Then, 10 is used as the input parameter of VMD and IMFs can be obtained as Fig. 9. The abscissa represents the time (s) and the ordinate represents the acceleration (m/s^2). SWT is performed on the 10 IMFs from VMD respectively to obtain the time-frequency distribution diagram (one of the time-frequency distribution diagrams is shown as Fig.10). We select the maximum norm of wavelet component as the instantaneous frequency of each discrete time (the blue line in Fig.10) and remove the low norm (we set 1×10^{-9} as the threshold, which means that when the norm is less than 1×10^{-9}, there is almost no vibration at this time, and the instantaneous frequency is 0).

After obtaining the instantaneous frequencies of all IMFs at each measurement point, we plot the instantaneous frequencies of all IMFs of three measurement points on the same diagram. Finally, we can obtain the instantaneous frequency lines of each IMF, as shown in Fig.11.

The abscissa in the figure indicates the frequency (Hz) and the ordinate represents the time (s). The blue dots in each column represent the instantaneous frequencies of every discrete time point of a certain IMF. If two columns of blue points are close to each other (i.e. the differences in frequency is less than 5Hz), we take the average value as the modal frequency. We also take the peak and valley of the power

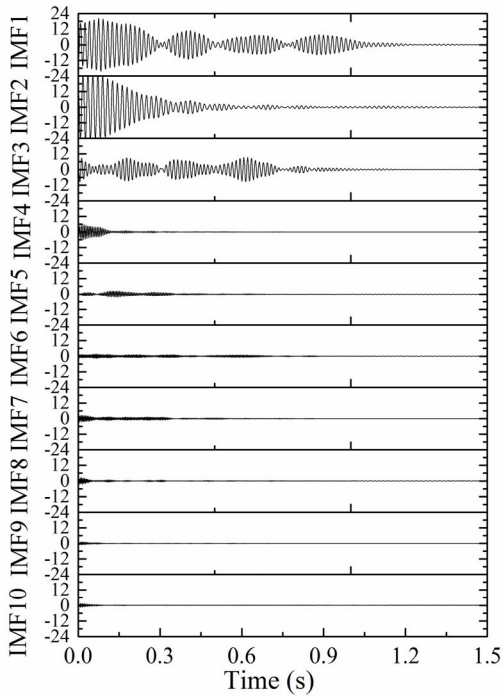

FIGURE 9. 10 IMFs obtained from VMD.

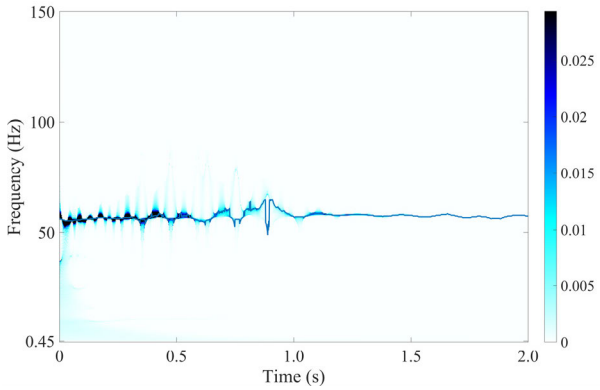

FIGURE 10. The time-frequency diagram of one IMF whose instantaneous frequency is about 60Hz.

spectrum curve into consideration. Since there are subjective errors when selecting the modal frequency and because of the error of the modal frequency identification itself, we think that an identified modal frequency differing from the theoretical result by less than 5% is the ideal result. The figure shows the following:

(1) The low-order modal frequencies of the rail are dense and only 11 orders of modal frequency can be identified. This is because the bending stiffness of the rail is lower than that of the fastener and the low-order modal frequency is mainly affected by the supporting stiffness.

(2) In condition 3, two instantaneous frequency bands occur around 30Hz. This is caused by the amplitude of the wheel-rail excitation 2 around 30Hz.

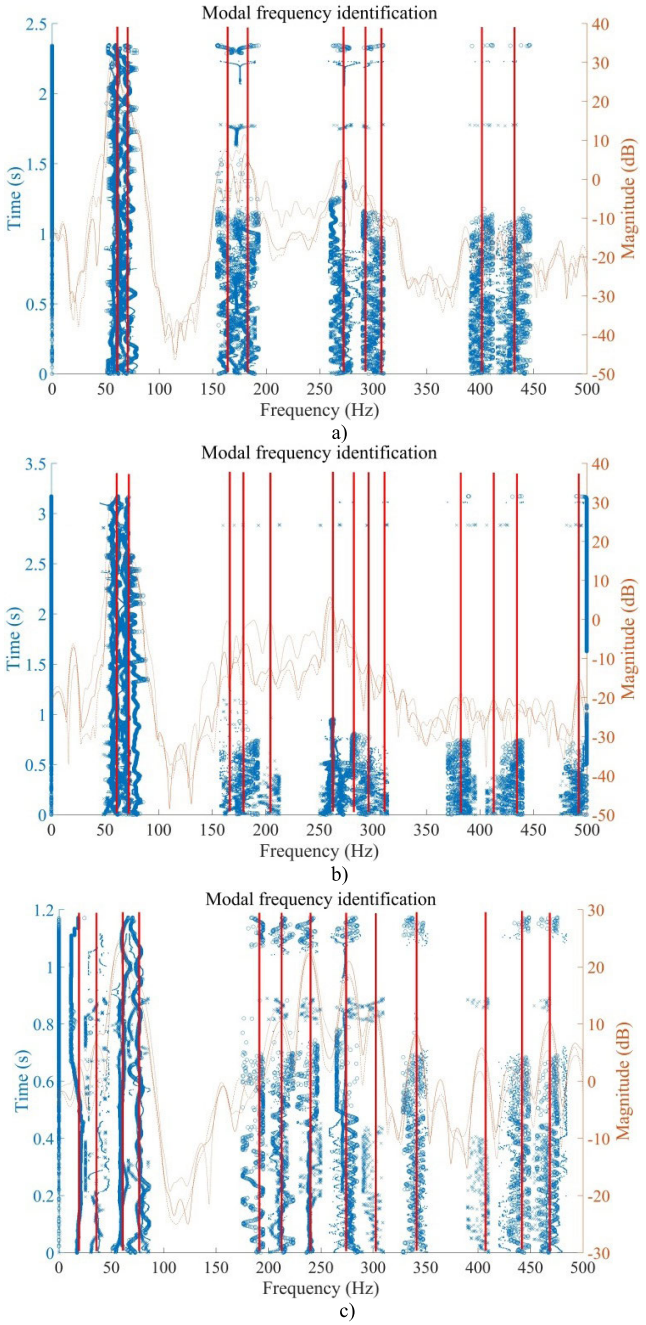

FIGURE 11. Modal frequency identification under condition 1 (a), condition 2 (b), and condition 3 (c).

(3) Two modal frequencies are close to each other near 70Hz and 165Hz. The frequency response curves of the rail near 65Hz and 165Hz are wide, and there are multiple modes in these two positions.

(4) In the range of 200∼300Hz, the number of modal frequencies identified by condition 1 and condition 2 is less than identified by condition 3. Wheel-rail excitation 2 has more energy in the high-frequency range; therefore, higher-order modal responses are larger and the frequencies are easier to identify.

(5) After 400Hz, there are still instantaneous frequency bands because the acceleration of the rail is mainly affected by the wheel-rail excitation.

The results of modal frequency identification and their comparisons with ERA identification results are shown in Table 3. We observe that there are still three orders of modal frequency that cannot be captured: 250Hz, 322Hz, and 338Hz. This may be due to the low wheel-rail excitation energy in high frequency, resulting in a low modal response in which VMD cannot decompose into IMFs. We analyze the influence of wheel-rail excitations in Section 4.

The deviation between them is shown in Fig.12. We observe from the figure that the modal frequency identified by wheel-rail excitation float above and below the modal frequency identified by the ERA method. In the low-order mode, the modal frequency identification deviation is up to 10% under a single calculation condition, but the average error is within 5%. In the high-order mode, the modal frequency deviations for the three calculation conditions are all within 5%, and the deviation of average results is further reduced.

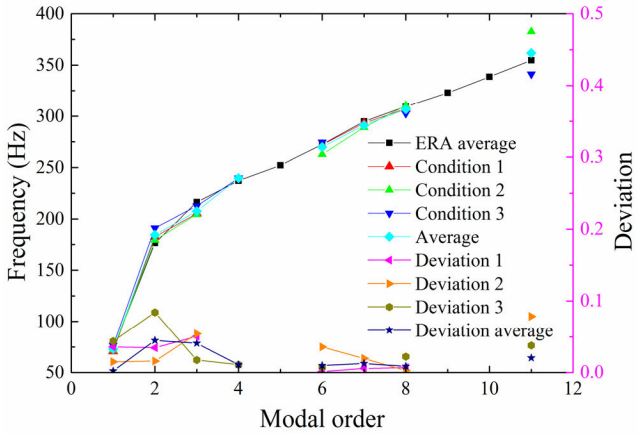

FIGURE 12. ERA method compared to MFIM.

The comparison shows that MFIM can effectively identify some modal frequencies of the rail from wheel-rail excitation.

IV. APPLICATION OF THE APPROACH

The original purpose of the proposed approach is to extract the modal frequency of the rail from the HSR monitoring system. Therefore, in this part, we study the influence of wheel-rail excitations and schemes of measuring point on the modal frequency identification results in the HSR ballastless track rail.

A. ESTABLISHMENT OF SLAB TRACK MODEL

The ballastless track model is shown in Fig.13. The equation of the rail and the fastener support force is the same as (22) and (23), respectively. The track slab is considered as a free beam on the elastic foundation and its equation is

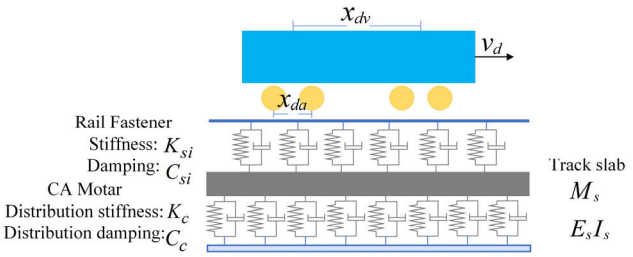

FIGURE 13. Ballastless track model.

expressed as:

$$M_s\ddot{S}_n(t) + c_cL_s\dot{S}_n(t) + (k_c + E_sI_s\beta_n^4) \times L_s \times S_n(t) = \sum_{j=1}^{N} F_{cbi}X_n(x_j) \quad (26)$$

where M_s is the mass of the track slab; c_c and k_c are the distribution damping and stiffness of the CA mortar, respectively; E_sI_s is the bending stiffness of the slab; β_n is a constant in the free beam mode function X_n [47]. L_s is the length of the track slab; S_n is the regular coordinate, and its equation is expressed as:

$$Z_{bi}(x,t) = \sum_{n=1}^{NMS} X_n(x)S_n(t) \quad (27)$$

Then, (22) and (26) can be written as:

$$\begin{aligned}
&\ddot{q}_k(t) + \sum_{i=1}^{N} C_{pi}Y_k(x_{wj}) \sum_{h=1}^{NM} Y_h(x_{wj})\dot{q}_h(t) + \frac{EI}{m_u}\left(\frac{k\pi}{l}\right)^4 q_k(t) \\
&\quad + \sum_{i=1}^{N} K_{pi}Y_k(x_{wj}) \sum_{h=1}^{NM} Y_h(x_{wj})q_h(t) \\
&\quad - \sum_{i=1}^{N} C_{pi}Y_k(x_{wj}) \sum_{n=1}^{NMS} X_n(x_i)\dot{S}_n(t) \\
&\quad - \sum_{i=1}^{N} K_{pi}Y_k(x_i) \sum_{n=1}^{NMS} X_n(x_i)S_n(t) = \sum_{j=1}^{4} p_j(t)Y_k(x_{wj}) \\
&\qquad (k = 1 \sim NM) \quad (28)
\end{aligned}$$

$$\begin{aligned}
&M_s\ddot{S}_n(t) + c_cL_s\dot{S}_n(t) + (k_c + E_sI_s\beta_n^4) \times L_s \times S_n(t) \\
&= \sum_{j=1}^{N}\Big(\sum_{h=1}^{NM} C_{pj}Y_h(x_{wj})\dot{q}_h(t) + \sum_{h=1}^{NM} K_{pj}Y_h(x_{wj})q_h(t) \\
&\quad - \sum_{h=1}^{NMS} C_{pj}X_h(x_{wj})\dot{S}_h(t) - \sum_{h=1}^{NMS} K_{pj}X_h(x_{wj})S_h(t)\Big)X_n(x_j) \\
&\qquad (n = 1 \sim NMS) \quad (29)
\end{aligned}$$

The parameters used in the model are shown in Table 4.

Five kinds of wheel-rail excitations (shown in Fig.14) with different spectral characteristics are used in the model. The moving speed of the excitations is 100 *m/s*. We extract dynamic responses at five random measuring points on the beam: $0.5l$ (above the fastener), $25.3125m$ (mid-span of

TABLE 4. Parameters used in the ballastless track model.

Parameter	Symbol	Value
Length of track	l	50 m
Mass per meter of rail	m_u	60 kg
Elastic modulus of rail	E	2.07e11 Pa
Inertia moment of rail	I	30.6e-6 m^4
Fastener spacing	x_{db}	0.625 m
Stiffness of fastener	K_{pi}	45000000N/m
Damping of fastener	C_{pi}	60000N·s/m
Elastic modulus of track slab	E_s	3.6×10^{10} Pa
Inertia moment of track slab	I_s	1.7×10^{-3} m^4
Mass of track slab	M_s	318750 kg
Distribution stiffness of CA mortar	K_c	255000000N/m^2
Distribution damping of CA mortar	C_c	2550000 N·s/m^2
Cutoff mode	NM	40

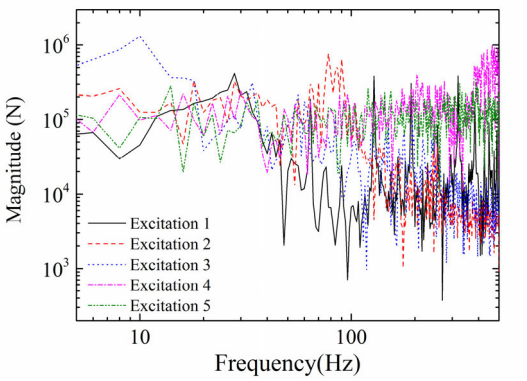

FIGURE 14. Frequecny-Magnitude diagram of wheel-rail excitations.

two fasteners), 25.15625m (quarter-span of two fasteners), 12.65625m, and 6.40625m, respectively.

B. INFLUENCE OF THE NUMBER OF WHEEL-RAIL EXCITATIONS AND MEASURING POINTS ON IDENTIFICATION RESULTS

We use the approach to process the rail acceleration extracted by five measuring points under five wheel-rail excitation conditions. The identification result is shown in Fig.15.

As can be seen from the figure, a total of eighteen order modal frequencies are identified. To study the influence of the number of measuring points and the number of wheel-rail excitations on the identification results, we show the results of using one measuring point to all five measuring points on Fig.16, and the results of using one wheel-rail excitation to all five excitations on Fig.17.

We observe from Fig.16 that one-order modal frequency cannot be identified using only one measuring point, but all the modal frequencies can be identified using two and more measuring points. When the number of measuring points is three, the deviation reduces to 1%.

As can be seen from Fig.17, all modal frequencies can be identified only if the number of wheel-rail excitations is

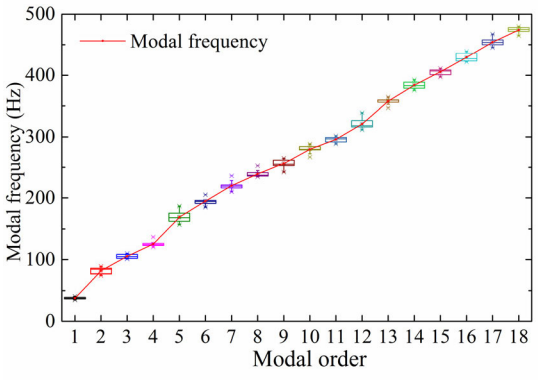

FIGURE 15. Modal frequency of the ballastless track rail.

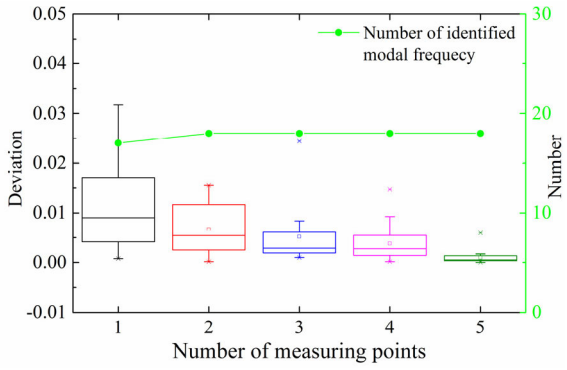

FIGURE 16. The influence of the number of measuring points.

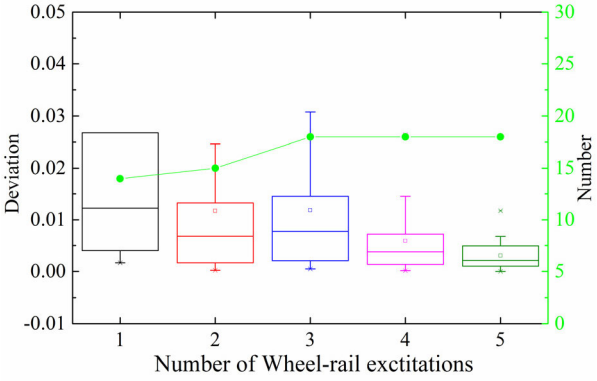

FIGURE 17. The influence of the number of wheel-rail excitations.

larger than three. When that number is four, the deviation reduces to 1%.

We can conclude from the above analysis that the number of wheel-rail excitations has a larger influence on the identification results. The more the rail response data under the different wheel-rail excitations obtained, the higher the accuracy of rail modal frequency identification. The number of measuring points has less influence than that of wheel-rail excitations on the modal frequency identification.

V. CONCLUSION

This paper proposes a novel approach for identifying the modal frequency of the track rail from wheel-rail excitation. The approach can extract the modal frequencies of the rail by using the vibration data from several measuring points on the rail. The paper validates the reliability of MFIM using a low vibration track model. Then this paper uses the approach to identify the modal frequencies of the HSR ballastless track rail and analyze the influence of the number of wheel-rail excitations and the number of measuring points on the identification results. It can be concluded that:

1) By using the rail acceleration after the wheel-rail excitations pass, the influence of the main frequencies of the wheel-rail forces on the rail acceleration can be effectively reduced, which is beneficial to the identification of the modal frequency of the track rail itself.
2) The difficulty of identifying high-order modal frequencies is relatively high, but the accuracy is greater. The deviation is basically within 5%, and via averaging the results identified using different operating conditions, a more accurate modal frequency can be obtained.
3) Compared with the number of measuring points, the number of wheel-rail excitations has a greater influence on the identification results. Considering the number of passing trains is large, therefore, 3∼4 rail measuring points meet the requirements of modal frequency identification.

ACKNOWLEDGMENT

The authors would like to thank the editor J. Lin and the reviewers for their helpful suggestions, which improved the quality of this review. The authors would also like to thank Ms. Y. Lv, Ms. Z. Ma and H. Jin for their kind discussions on this article.

REFERENCES

[1] J. Nielsen, A. Ekberg, and R. Lunden, "Influence of short-pitch wheel/rail corrugation on rolling contact fatigue of railway wheels," *Proc. Inst. Mech. Eng. F, J. Rail Rapid Transit*, vol. 219, no. 3, pp. 177–187, 2005, doi: 10.1243/095440905X8871.

[2] S. Mohammadzadeh, S. Ahadi, and M. Nouri, "Stress-based fatigue reliability analysis of the rail fastening spring clip under traffic loads," *Latin Amer. J. Solids Struct.*, vol. 11, no. 6, pp. 993–1011, Nov. 2014, doi: 10.1590/S1679-78252014000600006.

[3] X. L. Cui, G. X. Chen, H. G. Yang, Q. Zhang, H. Ouyang, and M. H. Zhu, "Study on rail corrugation of a metro tangential track with cologne-egg type fasteners," *Vehicle Syst. Dyn.*, vol. 54, no. 3, pp. 353–369, Mar. 2016, doi: 10.1080/00423114.2015.1137955.

[4] J. I. Egana, J. Vinolas, and M. Seco, "Investigation of the influence of rail pad stiffness on rail corrugation on a transit system," *Wear*, vol. 261, no. 2, pp. 216–224, Jul. 2006, doi: 10.1016/j.wear.2005.10.004.

[5] P. Vila, L. Baeza, J. Martinez-Casas, and J. Carballeira, "Rail corrugation growth accounting for the flexibility and rotation of the wheel set and the non-Hertzian and non-steady-state effects at contact patch," *Vehicle Syst. Dyn.*, vol. 521, no. 1, pp. 92–108, 2014, doi: 10.1080/00423114.2014.881513.

[6] L. Liu, X. Wang, Y. Zhou, and J. Qin, "Vibration mitigation effect investigation of a new slab track plate design," *Sensors*, vol. 19, no. 1, p. 1681, 2019, doi: 10.3390/s19010168.

[7] B. Jiang, M. Ma, M. Li, W. Liu, and T. Li, "Experimental study of the vibration characteristics of the floating slab track in metro turnout zones," *Proc. Inst. Mech. Eng. F, J. Rail Rapid Transit*, vol. 233, no. 10, pp. 1081–1096, 2019, doi: 10.1177/0954409719826824.

[8] W. Liu, H. Zhang, W. Liu, and D. J. Thompson, "Experimental study of the treatment measures for rail corrugation on tracks with egg fasteners in the Beijing metro," *Proc. Inst. Mech. Eng. F, J. Rail Rapid Transit*, vol. 232, no. 5, pp. 1360–1374, 2018, doi: 10.1177/0954409717721635.

[9] S. Kaewunruen and A. M. Remennikov, "Experimental simulation of the railway ballast by resilient materials and its verification by modal testing," *Exp. Techn.*, vol. 32, no. 4, pp. 29–35, Jul. 2008, doi: 10.1111/j.1747-1567.2007.00298.x.

[10] S. Kaewunruen and A. M. Remennikov, "Field trials for dynamic characteristics of railway track and its components using impact excitation technique," *NDT&E Int.*, vol. 40, no. 7, pp. 510–519, Oct. 2007, doi: 10.1016/j.ndteint.2007.03.004.

[11] X. Lei and C. Jiang, "Analysis of vibration reduction effect of steel spring floating slab track with finite elements," *J. Vib. Control*, vol. 22, no. 6, pp. 1462–1471, Apr. 2016, doi: 10.1177/1077546314539372.

[12] L. Baeza and H. Ouyang, "A railway track dynamics model based on modal substructuring and a cyclic boundary condition," *J. Sound Vib.*, vol. 330, no. 1, pp. 75–86, Jan. 2011, doi: 10.1016/j.jsv.2010.07.023.

[13] B. Liu, J. Lin, L. Zhang, and U. Kumar, "A dynamic prescriptive maintenance model considering system aging and degradation," *IEEE Access*, vol. 7, pp. 94931–94943, 2019, doi: 10.1109/ACCESS.2019.2928587.

[14] L. Hermans and H. Van der Auweraer, "Modal testing and analysis of structures under operational conditions: Industrial applications," *Mech. Syst. Signal Process.*, vol. 13, no. 2, pp. 193–216, Mar. 1999, doi: 10.1006/mssp.1998.1211.

[15] F. Ubertini, C. Gentile, and A. L. Materazzi, "Automated modal identification in operational conditions and its application to bridges," *Eng. Struct.*, vol. 46, pp. 264–278, Jan. 2013, doi: 10.1016/j.engstruct.2012.07.031.

[16] J. M. W. Brownjohn, F. Magalhaes, E. Caetano, and A. Cunha, "Ambient vibration re-testing and operational modal analysis of the Humber bridge," *Eng. Struct.*, vol. 32, no. 8, pp. 2003–2018, Aug. 2010, doi: 10.1016/j.engstruct.2010.02.034.

[17] E. Reynders and G. De Roeck, "Reference-based combined deterministic-stochastic subspace identification for experimental and operational modal analysis," *Mech. Syst. Signal Process.*, vol. 22, no. 3, pp. 617–637, Apr. 2008, doi: 10.1016/j.ymssp.2007.09.004.

[18] B. H. Kim, J. Lee, and D. H. Lee, "Extracting modal parameters of high-speed railway bridge using the TDD technique," *Mech. Syst. Signal Process.*, vol. 24, no. 3, pp. 707–720, Apr. 2010, doi: 10.1016/j.ymssp.2009.11.010.

[19] W. Yan and W. Ren, "Operational modal parameter identification from power spectrum density transmissibility," *Comput.-Aided Civil Inf.*, vol. 27, no. 3, pp. 202–217, Mar. 2012, doi: 10.1111/j.1467-8667.2011.00735.x.

[20] Y. B. Yang, B. Zhang, Y. Chen, Y. Qian, and Y. Wu, "Bridge damping identification by vehicle scanning method," *Eng. Struct.*, vol. 183, pp. 637–645, Mar. 2019, doi: 10.1016/j.engstruct.2019.01.041.

[21] Y. B. Yang, Y. C. Li, and K. C. Chang, "Constructing the mode shapes of a bridge from a passing vehicle: A theoretical study," *Smart Struct. Syst.*, vol. 13, no. 5, pp. 797–819, May 2014, doi: 10.12989/sss.2014.13.5.797.

[22] Y. B. Yang and J. D. Yau, "Resonance of high-speed trains moving over a series of simple or continuous beams with non-ballasted tracks," *Eng. Struct.*, vol. 171, pp. 1052–1053, Sep. 2018, doi: 10.1016/j.engstruct.2017.06.032.

[23] C. Tan, N. Uddin, E. J. O'Brien, P. J. McGetrick, and C. Kim, "Extraction of bridge modal parameters using passing vehicle response," *J. Bridge Eng.*, vol. 24, no. 9, 2019, Art. no. 04019087, doi: 10.1061/(ASCE)BE.1943-5592.0001477.

[24] H. Li, S. Li, J. Ou, and H. Li, "Modal identification of bridges under varying environmental conditions: Temperature and wind effects," *Struct. Control Health Monit.*, vol. 17, no. 5, pp. 495–512, 2010, doi: 10.1002/stc.319.

[25] J. M. W. Brownjohn, S.-K. Au, Y. Zhu, Z. Sun, B. Li, J. Bassitt, E. Hudson, and H. Sun, "Bayesian operational modal analysis of Jiangyin Yangtze river bridge," *Mech. Syst. Signal Process.*, vol. 110, pp. 210–230, Sep. 2018, doi: 10.1016/j.ymssp.2018.03.027.

[26] B. Peeters, H. Van der Auweraer, F. Vanhollebeke, and P. Guillaume, "Operational modal analysis for estimating the dynamic properties of a stadium structure during a football game," *Shock Vib.*, vol. 14, no. 4, pp. 283–303, 2007, doi: 10.1155/2007/531739.

[27] L. F. Ramos, L. Marques, P. B. Lourenco, G. De Roeck, A. Campos-Costa, and J. Roque, "Monitoring historical masonry structures with operational modal analysis: Two case studies," *Mech. Syst. Signal Process.*, vol. 24, no. 5SI, pp. 1291–1305, Jul. 2010, doi: 10.1016/j.ymssp.2010.01.011.
[28] D. Uehara and J. Sirohi, "Full-field optical deformation measurement and operational modal analysis of a flexible rotor blade," *Mech. Syst. Signal Process.*, vol. 133, p. 106265, Nov. 2019, doi: 10.1016/j.ymssp.2019.106265.
[29] X. Jiang, B. Li, X. Mao, Y. Peng, and S. He, "New approach based on operational strain modal analysis to identify dynamical properties of the high-speed reciprocating operation mechanism," *J. Freq. Noise, Vib. Act. Control*, vol. 38, nos. 3–4, pp. 1345–1362, Dec. 2019, doi: 10.1177/1461348418821203.
[30] H. Lam, J. Yang, and J. L. Beck, "Bayesian operational modal analysis and assessment of a full-scale coupled structural system using the Bayes-mode-ID method," *Eng. Struct.*, vol. 186, pp. 183–202, May 2019, doi: 10.1016/j.engstruct.2019.02.016.
[31] S. Au and J. M. W. Brownjohn, "Asymptotic identification uncertainty of close modes in Bayesian operational modal analysis," *Mech. Syst. Signal Process.*, vol. 133, p. 106273, Nov. 2019, doi: 10.1016/j.ymssp.2019.106273.
[32] Y. Xin, H. Hao, and J. Li, "Time-varying system identification by enhanced empirical wavelet transform based on synchroextracting transform," *Eng. Struct.*, vol. 196, p. 109313, Oct. 2019, doi: 10.1016/j.engstruct.2019.109313.
[33] L. W. Zhang, J. Lin, B. Liu, Z. C. Zhang, X. H. Yan, and M. H. Wei, "A review on deep learning applications in prognostics and health management," *IEEE Access*, vol. 7, pp. 162415–162438, 2019, doi: 10.1109/ACCESS.2019.2950985.
[34] H. Shao, H. Jiang, H. Zhang, and T. Liang, "Electric locomotive bearing fault diagnosis using a novel convolutional deep belief network," *IEEE Trans. Ind. Electron.*, vol. 65, no. 3, pp. 2727–2736, Mar. 2018, doi: 10.1109/TIE.2017.2745473.
[35] V. J. Hodge, S. O'Keefe, M. Weeks, and A. Moulds, "Wireless sensor networks for condition monitoring in the railway industry: A survey," *IEEE Trans. Intell. Transp.*, vol. 16, no. 3, pp. 1088–1106, Jun. 2015, doi: 10.1109/TITS.2014.2366512.
[36] D. Barke and W. K. Chiu, "Structural health monitoring in the railway industry: A review," *Struct. Health Monit.*, vol. 4, no. 1, pp. 81–93, Mar. 2005, doi: 10.1177/1475921705049764.
[37] B. Liu, P. Do, B. Iung, and M. Xie, "Stochastic filtering approach for condition-based maintenance considering sensor degradation," *IEEE Trans. Autom. Sci. Eng.*, to be published, doi: 10.1109/TASE.2019.2918734.
[38] K. Dragomiretskiy and D. Zosso, "Variational mode decomposition," *IEEE Trans. Signal Process.*, vol. 62, no. 3, pp. 531–544, Feb. 2014, doi: 10.1109/TSP.2013.2288675.
[39] Q. Chen, X. Lang, L. Xie, and H. Su, "Detecting nonlinear oscillations in process control loop based on an improved VMD," *IEEE Access*, vol. 7, pp. 91446–91462, 2019, doi: 10.1109/ACCESS.2019.2925861.
[40] P. Ni, J. Li, H. Hao, Y. Xia, X. Wang, J.-M. Lee, and K.-H. Jung, "Time-varying system identification using variational mode decomposition," *Struct. Control Health Monit.*, vol. 25, no. 6, p. e21756, Jun. 2018, doi: 10.1002/stc.2175.
[41] I. Daubechies, J. Lu, and H. T. Wu, "Synchrosqueezed wavelet transforms: An empirical mode decomposition-like tool," *Appl. Comput. Harmon. Anal.*, vol. 30, no. 2, pp. 243–261, Mar. 2011, doi: 10.1016/j.acha.2010.08.002.
[42] K. He and X. Li, "Time-frequency feature extraction of acoustic emission signals in aluminum alloy MIG welding process based on SST and PCA," *IEEE Access*, vol. 7, pp. 113988–113998, 2019, doi: 10.1109/ACCESS.2019.2935117.
[43] Q. Jiang and B. W. Suter, "Instantaneous frequency estimation based on synchrosqueezing wavelet transform," *Signal Process.*, vol. 138, pp. 167–181, Sep. 2017, doi: 10.1016/j.sigpro.2017.03.007.
[44] C. Esveld, *Modern Railway Track*, 6th ed. Beijing, China: China Railway Publishing House, 2014, pp. 106–168.
[45] L. Gao, "Track engineering," in *Track Structure Mechanics Analysis*, 5th ed. Beijing, China: China Railway Publishing House, 2010, pp. 154–176.
[46] J. N. Juang and R. S. Pappa, "An eigensystem realization algorithm for modal parameter identification and model reduction," *J. Guid. Control Dyn.*, vol. 8, no. 5, pp. 620–627, Sep. 1985, doi: 10.2514/3.20031.
[47] W. M. Zhai, *Vehicle Track Coupling Dynamics*, vol. 1, 2nd ed. Beijing, China: Science Press, 2015, pp. 11–94.

BOLUN AN received the B.S. degree from the Henan University of Technology, Zhengzhou, China, in 2015. He is currently pursuing the Ph.D. degree in highway and railway engineering with the School of Civil Engineering, Beijing Jiaotong University, Beijing, China. His research interests include high-speed railway track operational modal parameters identification and track dynamics.

LIANG GAO received the B.S., M.S., and Ph.D. degrees from Southwest Jiaotong University, Chengdu, China, in 1990, 1993, and 1997, respectively. Since 2004, he has been a Professor with the School of Civil Engineering, Beijing Jiaotong University. He is the author of 16 books, more than 180 articles, and holds more than 20 patents. His research interests include the new-type track structure, track dynamics, continuously welded rails in high-speed railways, and the structural health monitoring of the railway system. He is a member of the Committee of China Railway Corporation, the Vice-Chairman of Standardization (Track) Technical Committee of China Railway Association, and the Director of the Railway Branch of China Engineering Construction Association. His awards and honors include the First Prize of the State Scientific and Technological Progress Award as the first prizewinner in 2017, the Scientific and Technological Progress Award of The Ho Leung Ho Lee Foundation in 2018, the National Ten-thousand Talents Program in 2018, the Chang Jiang Scholars Programme of Ministry of Education in 2014, the "Science and Technology Beijing" 100 Leading Talents Training Project in 2018, and the Chinese University's Top 10 Scientific and Technological Advances Award in 2013.

TAO XIN received the B.S. and Ph.D. degrees from Beijing Jiaotong University. He is currently a Professor with the Department of Road and Railway Engineering, Beijing Jiaotong University. He is also a Key Member of the Beijing Key Laboratory of Track Engineering. His research interests include wheel/rail contact problem and vibration reduction technology in rail transit.

GUORONG XIANG received the B.S. degree in civil engineering from Beijing Jiaotong University, Beijing, China, in 2014, where he is currently pursuing the master's degree in highway and railway engineering. His research interest includes ballastless track and modal analysis.

JI WANG received the B.S. degree in railway engineering and the M.S. degree in highway and railway engineering from Beijing Jiaotong University, Beijing, China, in 2016 and 2018, respectively. He is currently pursuing the Ph.D. degree in highway and railway engineering with the Key Laboratory of Track Engineering, Beijing Jiaotong University. His research interests include ballastless railway track and materials in the railway track.